Organs-on-a-Chip 4 (2022) 100024

Contents lists available at ScienceDirect

Organs-on-a-Chip

journal homepage: www.sciencedirect.com/journal/organs-on-a-chip

The tumour microenvironment modulates cancer cell intravasation

Ayushi Agrawal [a], Somayeh Shahreza [a], Yousef Javanmardi [a], Nicolas Szita [b], Emad Moeendarbary [a,c,*]

[a] Department of Mechanical Engineering, University College London, London, WC1E 7JE, UK
[b] Department of Biochemical Engineering, University College London, London, WC1E 7JE, UK
[c] Department of Biological Engineering, Massachusetts Institute of Technology, Cambridge, MA, 02139, USA

ARTICLE INFO

Keywords:
Intravasation
Extracellular matrix
Composite hydrogels
Tumour spheroids
Microvasculature
Microfluidics

ABSTRACT

Development of three dimensional (3D) *in vitro* models to realistically recapitulate tumor microenvironment has the potential to improve translatability of anti-cancer drugs at the preclinical stage. To capture the *in vivo* complexity, these *in vitro* models should minimally incorporate the 3D interactions between multiple cell types, cellular structures such as vasculature and extracellular matrices. Here, we utilised microfluidic platforms to study the effect of various natural hydrogels (fibrin, collagen, Matrigel) and presence of tumor spheroids on the 3D vascularisation morphology. Various extracellular matrix (ECM) compositions impacted the vessel morphology while near the tumor spheroids the vessel diameter was considerably smaller for all different ECM compositions. Strikingly, cancer cells could enter the microvessel lumens (i.e. intravasate) only when the ECM was comprised of all the three types of hydrogels which increased the physical contact between the microvessels and the tumour spheroids. Our findings highlight the role of ECM composition in modulating the intravasation capacity of tumours.

1. Introduction

The majority of deaths in solid tumours is due to metastasis (Ahmad and Anderson, 2021; Dillekås et al., 2019) which is defined as the physical movement of cancer cells from their primary site of origin to a distant organ. To disseminate, cancer cells must traverse through several physical barriers in a series of steps, including invasion through the surrounding tissue, infiltration into the nearest blood vessel (intravasation), transportation to a secondary organ through circulation, followed by extravasation and colonisation at the secondary site (Fokas et al., 2007; Roberts et al., 2021). Amongst this multi-step process, intravasation is considered as a rate-limiting step in the metastatic cascade as it regulates the quantity of circulating tumour cells that act as potential metastatic seeds (Zervantonakis et al., 2012). Thus, targeting this event offers the potential to curb the spread of cancer cells and contain it at its primary site, which can be surgically treated. However, a major drawback to achieve this approach is the current technological limitations at the preclinical stage, particularly lack of robust *in vitro* assays for testing of anti-cancer drugs targeting specific stages of metastasis (Mak et al., 2014; Chen et al., 2018). Thus, the need for the creation of advanced *in vitro* platforms that utilise cells of human origin as well as mimic the complexity of 3D tumour microenvironment (TME) has escalated.

Although the mechanisms of cancer cell intravasation have been widely understood, there are only a few *in vitro* models that recapitulated this event. These include boyden/transwell assays (Li and Zhu, 1999), artificial microvessels (Naserian et al., 2019), tissue culture dishes (Ehsan et al., 2014), 3D printing (Meng et al., 2019) and microfluidics (Zervantonakis et al., 2012; Han et al., 2016; Whelan et al., 2021) that have been developed to mimic the pathophysiology of the TME. These *in vitro* models utilise an endothelial monolayer to observe cancer cell transmigration across 2D endothelium which is an oversimplified assumption of infinite flat plane of endothelial cells representing 3D microvascular networks (Haase and Kamm, 2017). As these monolayers are unable to recapitulate the correct geometrical and polarity of endothelial cells (luminal and abluminal) (Dua et al., 2005; Tacconi et al., 2022), several attempts have been made to create *in vitro* models of 3D vascularised tumours. These vascularised models show considerable improvement in recapitulating the cellular tumour microenvironment and mimicking the preliminary steps of intravasation (Haase et al., 2020; Michna et al., 2018; Nashimoto et al., 2020; Maggeldin et al., 2017). However, to our knowledge, they were unable to

* Corresponding author. University College LondonDepartment of Mechanical Engineering Roberts Engineering Building Torrington Place, London, WC1E 7JE, UK.
E-mail address: e.moeendarbary@ucl.ac.uk (E. Moeendarbary).

https://doi.org/10.1016/j.ooc.2022.100024
Received 15 December 2021; Received in revised form 15 October 2022; Accepted 15 October 2022
Available online 22 October 2022

capture appropriate complexity needed for the escape of cancer cells into the microvessel lumens. While these previous vascularised tumor models have successfully recreated the spatial confinement of cells in 3D, the lack of appropriate ECM composition can be a potential reason for their ineffectiveness to capture intravasation events (Cox, 2021).

The choice of a hydrogel with appropriate physical and biochemical characteristics relevant to *in vivo* TME is of utmost importance. The ECM is incorporated in 3D *in vitro* models in the form of biocompatible hydrogels, acting as a scaffold to embed cells to create 3D spatial organisations (Lee et al., 2017). A few groups have shown that the use of a single hydrogel as a representative of the complex TME does not necessarily recapitulate the appropriate chemical and mechanical aspects of the TME, which in turn regulate cell-cell and cell-ECM interactions (Hong and Stegemann, 2008; Lai et al., 2012; Anguiano et al., 2017, 2020). Therefore, composite matrices made from a combination of hydrogels offer significant advantage of collating proteins, growth factors and biomechanical cues relevant to TME. So far, to our knowledge, this approach has not yet been exploited for mimicking the process of cancer intravasation *in vitro*.

Here, we performed a comparative study on the effect of matrix composition on microvascular network formation in the presence and absence of 3D tumour spheroids, utilising microfluidic platform. We employ two hydrogel combinations, collagen and Matrigel, mixed with the widely used blood clotting protein, fibrin that has been widely used for the formation of 3D self-assembled microvascular networks. Collagen is chosen as it forms the most abundant fibrous protein component of the ECM (Cox, 2021), while Matrigel from the ECM of an EHS mouse sarcoma is rich in basement membrane proteins (such as laminin, collagen IV, fibronectin, entactin) of epithelial cells in addition to, containing growth factors essential for tumour growth (Ye and Qiu, 2019). Consequently a mixture of all of these three hydrogels is of particular interest, as it combines structural features of collagen, bioactive properties of Matrigel and fibrin hydrogel, an integral component of vascular tissue engineering scaffolds and known modulator of tumour growth and metastasis (Kwaan and Lindholm, 2019). We further demonstrate the advantage of using the combination of these hydrogels to generate a new intravasation assay for solid tumours.

2. Material and methods

2.1. Device design and mould fabrication

The device comprising three parallel channels (3 mm wide, 11 mm long, 1 mm high), feature the gel channel separated by two adjacent media channels. The gel channel was delineated from the media channels by micro pillars separated by ~200 μm gaps. 2 mm and 3 mm inlet and outlet ports were connected to the hydrogel and media channels respectively. CAD drawing was used to design the pattern of the device (see supplementary file). Laser cutter (Epilog) was used to cut the pattern through a 1 mm thick PMMA sheet. To fabricate the fine features of the micropillars, the laser was etched multiple times at low power and speed modes. A plate of acrylic sheet was printed using the cutter to be used as a base for the mould. The mould and base plate were bonded together with acrylic cement (Scigrip Weld On 4SC).

2.2. Device fabrication

Microfluidic devices were fabricated out of polydimethylsiloxane (PDMS, Sylgard, Dow Corning). To fabricate devices, PDMS and curing agent were mixed in a ratio 10:1. The mixture was degassed using a desiccator for about 20 min or until the bubbles disappear. Then, the degassed PDMS was poured over the mould and cured in a pre-warmed oven at 80° C for 90 min. Using a scalpel, the cured PDMS device was detached and peeled off very gently. Ports of diameter 2 mm and 3 mm were punched for the gel and media channels respectively using biopsy punches. The fabricated device was cleaned with a residue-free tape and autoclaved to sterilise. A clean glass coverslip (Electron Microscopy Science) and the device were bonded using a plasma gun (Blackhole. LAB). The bonded devices were kept in an oven at 80° C to restore hydrophobicity.

2.3. Cell culture

Green Fluorescent Protein expressing Human Umbilical Vein Endothelial Cells (GFP-HUVECs, 2B Scientific) were cultured in Endothelial Growth Medium (EGM-2MV, Lonza) and passaged 6 to 8 times for the experiments. Normal Human Lung Fibroblasts (NHLF, Lonza) were cultured in Fibroblast Growth Medium (FGM-2, Lonza) and used up to passage 8 for all experiments. Human colorectal adenocarcinoma (HT29, Sigma) cells were cultured in McCoys 5A medium (Sigma) supplemented with 10% FBS and 1% penicillin-streptomycin solution. HT29 cells were transduced with a recombinant lentivirus harbouring LifeAct®-TagRFP transgene (Ibidi, Germany) for visualisation purposes. Human lung cancer cell line (A549, Sigma) was cultured in F–12K medium (Thermo Fisher Scientific) supplemented with 10% FBS and 1% penicillin-streptomycin solution.

2.4. Spheroid formation

HT29 and A549 cells were disassociated from culture dish using trypsin-EDTA (0.05%, HyClone), spun-down and counted (10,000 cells/well). The cells were resuspended in their growth medium supplemented with 20% Methocel solution and seeded about 100μl/well in a 96 well U-bottom plate. The plate was then, centrifuged at 350 rcf for 10 min and incubated in an incubator at 37°C, 5% CO_2 afterwards. The spheroids were harvested for seeding in the microfluidic device after 4 days.

2.5. Hydrogel preparation

Fibrin hydrogel was prepared by mixing equal volumes of thrombin and fibrinogen solution. Fibrinogen solution was prepared by reconstituting 6 mg/ml bovine fibrinogen (Sigma) in PBS without calcium and magnesium in a water bath at (37°C) for 2 h. The solution was then, filter sterilised and stored at 4°C and used within a week. Thrombin stock solution was prepared by dissolving thrombin (1KU, Sigma) in 10 ml PBS without calcium and magnesium. This mixture was filter sterilised and aliquots were stored at −20°C for up to 6 months. The working thrombin solution (4U/ml) was prepared in EGM-2MV media over ice.

Collagen hydrogel was prepared by using pre-cooled sterile water, HEPES buffer, 10x PBS-phenol red, NaOH (0.5 M) and rat-tail Collagen I (VWR International). These solutions were mixed such that the working collagen I concentration to be 2 mg/ml at pH 7.4. The mixture was prepared fresh for each experiment.

Growth factor reduced Matrigel® (Corning) was aliquoted and stored at −20°C.

2.6. Cell seeding

All the cell seeding procedures were done over ice. GFP-HUVECs (16x10^6/ml) and NHLFs (8x10^6/ml) (Mak et al., 2014) were disassociated and counted. Equal amounts of GFP-HUVECs and NHLF suspensions were gently mixed and centrifuged to pellet the cells and resuspend in thrombin working solution. The cells suspension in thrombin was mixed with equal volume of fibrinogen solution to achieve a final concentration of 4x10^6 GFP-HUVECs/ml and 2x10^6 NHLFs/ml and immediately injected into the gel channel. The seeded devices were placed in a humidity box and incubated at room temperature for 30 min, before filling the media channels with pre-warmed EGM-2MV media. The microfluidic devices were kept in the incubator (37°C, 5% CO_2) and media was exchanged every 24 h.

The above-mentioned protocol is for the case of cells embedded in pure fibrin hydrogel. Other combinations of hydrogels are with

volumetric ratios of: Fibrin:Collagen (1:1), Fibrin:Matrigel (1:1), Fibrin: Collagen:Marigel (2:1:1). For example, to prepare F:C:M hydrogel, equal volumes of fibrinogen, thrombin, collagen and Matrigel were mixed with the cell mixture. Thus, the final concentration of each hydrogel combination injected into microfluidic channel is F:C (Fibrin 1.5 mg/ml, Collagen 1 mg/ml), F:M (Fibrin 1.5 mg/ml, Matrigel 3.65 mg/ml), F:C:M (Fibrin 1.5 mg/ml, Collagen 0.5 mg/ml, Matrigel 1.8 mg/ml). To co-culture tumour spheroids embedded within vascular networks, HT29 spheroids were removed from the 96-well plate and resuspended in thrombin working solution, before mixing with the appropriate hydrogel-cell mixture, resulting in a final concentration of 4x10^6 GFP-HUVECs/ml and 2x10^6 NHLFs/ml.

2.7. Microvessel perfusion test and quantification

Dextran perfusion test is a simple measure of the degree of lumens interconnectivity. The perfusion of microvascular networks was checked by injecting fluorescently labelled 70 kDa blue dextran (Sigma) through one of the media channels. Briefly, media from both media channels was aspirated and dextran was introduced in one channel, this creates a pressure difference across the hydrogel channel, directing the flow of dextran through the hydrogel.

For perfusability quantification, the percentage of microvessel lumens containing dextran after perfusion was assessed. Both the endothelial cells and dextran channels images were binarised and the perfused area within the microvessels was calculated. The percentage perfusability was calculated by dividing the area of the vessels filled with dextran to the total area of the vessels.

2.8. Immunostaining

Hoechst33342 (1:1000 μl, New England Biolabs) and Hu CD31 Alexa 647 (5:100 μl, BD BioScience) were used to stain the nuclei and platelet endothelial cell adhesion molecule-1 (PECAM-1), respectively. To stain, the media was aspirated, and the working solutions were introduced to one of the 2 side channels and incubated for 10 min. The solutions can then be removed and washed with PBS (3 times, with 5 min intervals).

2.9. Imaging and image quantification

All images were captured by a confocal microscope (Olympus FV1000) with 10X, 20X, 40X and 60X objectives (Olympus). For image quantification, microvessels diameter and microvessels coverage area were analysed using ImageJ (Fiji) and for orthogonal projections IMARIS (Bitplane) was used.

To measure microvessels diameter, 3D confocal z-stack images were projected on a plane. The diameters were then measured manually by drawing a line from one edge of a microvessel to another edge. The length of the lines was measured using ImageJ. Similar steps were performed to evaluate the distance between spheroid edge and nearest microvessel wall. To quantify the microvessels coverage area, the area covered by the microvasculature in an image was divided by the total area of the image. For this, only GFP-HUVECs channel was processed by reducing the background noise, followed by thresholding, binarising, and using "Analyse Particle" plugin in ImageJ.

To measure the intravasation rates, we tracked the number of cancer cells that entered each lumen per spheroid by manually counting the cells from confocal z-stack images. The shape of spheroids was considered ellipsoid with volume calculated using major and minor axes on xy plane, and the height at day 7. The number of intravasated cells per lumen were divided to the spheroid volume at day 7 to estimate the intravasation rates at days 7, 10, and 12.

3. Results

3.1. Formation and characterisation of in vitro microvascular networks in composite matrices

In order to understand the effect of matrix composition on the microvascular network formation, we employed a widely used microfluidic platform (Haase et al., 2020). Briefly, the microfluidic device comprises of three channels - a central gel channel and two adjacent media channels. HUVECs and NHLFs were encapsulated in the gel channel with appropriate 3D ECM hydrogel (Fig. 1 a, b, c). The hydrogel combinations we chose were Fibrin:Collagen (F:C = 1:1), Fibrin:Matrigel (F:M = 1:1), and Fibrin:Collagen:Matrigel (F:C:M = 2:1:1), where the ratios are volumetric. The cells begin to spread, adhere to the ECM and reorient within the gel, with HUVECs organising into vessel-like interconnected structures by day 4 which gradually matures by day 7, in the presence of stromal cells. We observed profoundly different spatial arrangement of the microvasculature in different microenvironment owing to alterations in the hydrogel composition (Fig. 1 d). Amongst the different combinations of Fibrin (F), Collagen (C) and Matrigel (M) hydrogels, the composite matrices had fixed fibrin content (1.5 mg/ml) for stable microvascular network formation. Significant difference in the vessel diameter was observed in the case of F:C and F:M with respect to fibrin hydrogel, while no-significant difference existed between F:C:M and F hydrogels (Fig. 1 e). The condition with F:C and F:M hydrogels had narrow microvessel diameter, seemed disorganised, and regressed soon after day 7, in comparison to microvessels in fibrin hydrogel. This observation is in agreement with the existence of perfusable microvessels in both F and F:C:M cases, while F:C and F:M hydrogels exhibited non-perfusable microvasculature (Supplementary Fig. 1). Similarly, significant differences were observed in the average vessel coverage area amongst the hydrogel combinations (Fig. 1 f), highlighting the importance of ECM in regulating cellular cross-talk.

4. Introduction of tumour spheroids and characterisation of tumour-specific impact on vascular morphogenesis

Since the hydrogel (collagen, Matrigel) constitutes part of the TME, we set out to understand its impact when spheroids are co-cultured with HUVECs and NHLFs. To achieve this, we integrated two commonly used 3D *in vitro* technology of spheroid generation and cell seeding in a suitable 3D microenvironment (Fig. 2 a, b). Following seven days in culture, prominent differences in tumour growth pattern and its interaction with the microvessels could be seen (Fig. 2 c) in different composite matrices. For the same concentration of cells seeded, we observed considerable differences in the distance between the edge of tumour spheroid and its nearest microvessels, with maximum distance between them occurring in the case of fibrin hydrogel, which gradually decreased with the introduction of physiologically relevant TME constituents (Fig. 2 d). As expected, the introduction of both matrigel, collagen in fibrin hydrogel (F:C:M case) led to enhanced physical contact between the spheroids and the microvessels, highlighting the benefit of increasing complexity in the ECM. The presence of cancer spheroid also reduced the average vessel diameter of the microvessels in proximity to spheroid, compared to the case with absence of spheroid embedded alongside the vasculature, for each corresponding matrix condition (Figs. 1 and 2 e). Moreover, the microvessel coverage area decreased significantly in F:C, F:M hydrogels, which was recovered in F:C:M case compared to fibrin only hydrogel (Fig. 2 f), signifying better recapitulation of TME in a composite F:C:M matrix.

5. Development of cancer cell intravasation assay

The addition of collagen or Matrigel individually to fibrin gel, despite reflecting better physical closeness to the microvessels showed reduced vessel density, reflecting the unique pro-tumorigenic properties that

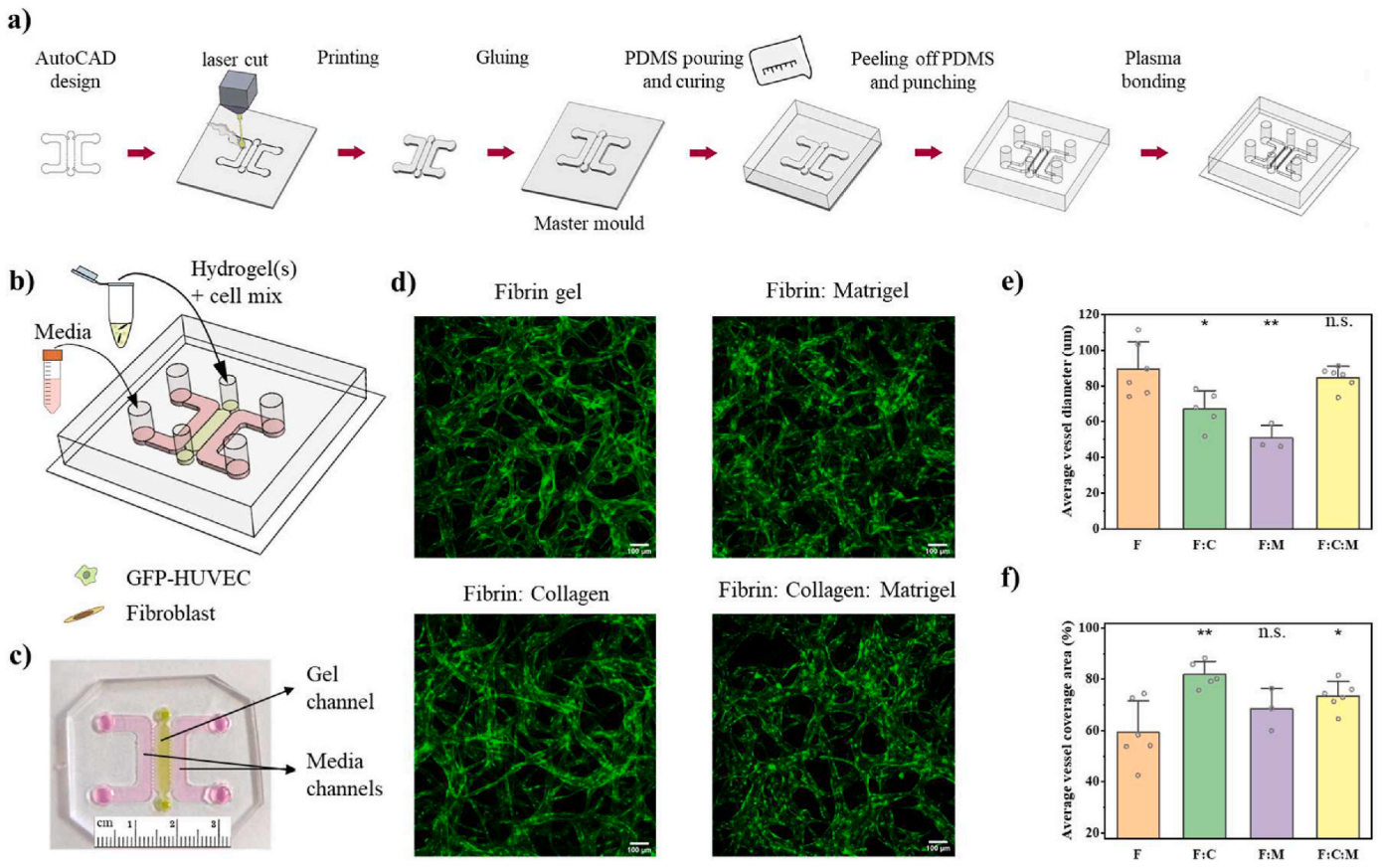

Fig. 1. Microvasculature morphogenesis in different hydrogel combinations – a) schematic representing mould and microfluidic device fabrication, b) encapsulation of GFP-HUVECs and fibroblasts in the microfluidic device, c) photograph of the top-view of the three-channel microfluidic device, d) microvasculature formation in different combinations of hydrogels at day 7 post seeding in the microfluidic device, e) graph representing the average vessel diameter in different hydrogel combinations at day 7, f) graph representing average coverage area of the microvasculature in different conditions at day 7. Data is represented as mean ± SD, with n = 6 for Fibrin, n = 5 for Fibrin:Collagen, n = 3 for Fibrin:Matrigel, n = 6 for Fibrin:Collagen:Matrigel, over 3 independent experiments. Statistical significance was tested with student's t-test (*p< 0.05, **p<0.01, n.s. p > 0.05).

each of them bring in the F:C:M case. This observation was strengthened when we observed cancer cell intravasation events only in F:C:M hydrogels, while the cancer cells would remain at the perivascular interface in all other matrix compositions, which led us to develop a new cancer cell intravasation assay (Fig. 3 a). Over the period of 7 days, we observed asymmetric growth of the tumour spheroid with strands of cancer cells invading through the ECM towards the nearest microvessels (Fig. 3 b, Supplementary Fig. 2). The microvascular networks around the spheroid were well-interconnected, perfusable, and functional (Fig. 3 b) as visible by dextran perfusability test. By day 7, we began to observe the infiltration of cancer cells into the microvessels. To confirm the entry of cancer cells in the lumens, we analysed the orthogonal projections of the z-stack images obtained from confocal microscope, to avoid confusion with the cancer cells that are located at the perivascular interface, as they can be easily misinterpreted as cancer cell intravasation events (Fig. 3 b). Then, to further characterise the events of intravasation, we performed time-lapse imaging at 40x to track the infiltrated cancer cells until day 12 and found the cancer cell shedding to be a dynamic process with more cells infiltrating every day (Fig. 3 e). The difference in cancer cell shedding is not significant, suggesting that the intravasation of cells is a gradual process. The penetration of cancer cells was mostly seen as collective clusters (ranging from 4 to 20 cells/cluster on day 12) instead of single CTCs (circulating tumour cells) amongst the intravasation events (Fig. 3 c). Interestingly, staining with CD31, also known as Platelet Endothelial Cell Adhesion Molecule-1 (PECAM-1), a universal marker of endothelium, revealed no discernible damage to inter-connected junctions of endothelial cells at the point of intravasation (Fig. 3 d) by the confocal microscope at 60x, suggesting such interactions maybe transient.

6. Concluding remarks

In this work, we exploited the microfluidic platform to control the TME factors, conduct high resolution imaging to successfully recapitulate cancer cell intravasation events. To capture TME complexity, we embedded multicellular 3D tumour spheroid in a composite matrix that contained stromal fibroblasts and endothelial cells to form perfusable microvasculature. To prove the efficacy of composite matrices, first we compared the change in morphology of the microvascular network in fibrin gel and its combination with collagen and Matrigel, each resembling specific features of the TME. We observed striking differences in the vessel diameter and vessel coverage area in various hydrogel combinations. The microvessels formed in F:C and F:M mixtures had narrow diameter, disorganised network, and were non-perfusable in comparison to F and F:C:M mixtures. This suggests that although collagen and Matrigel individually represents the major components of interstitial and basement membrane respectively (Han et al., 2016), their combination is a better representative of the TME.

We then, introduced tumour spheroids along with endothelial cells and stromal fibroblasts in the microfluidic device to study how tumour spheroids integrate into TME during vascularisation of composite hydrogel. Interestingly, we found a considerable decrease in the distance between the spheroid edge and the nearest microvessels when using more complex mixture of hydrogels (Fig. 2 d). A void region of

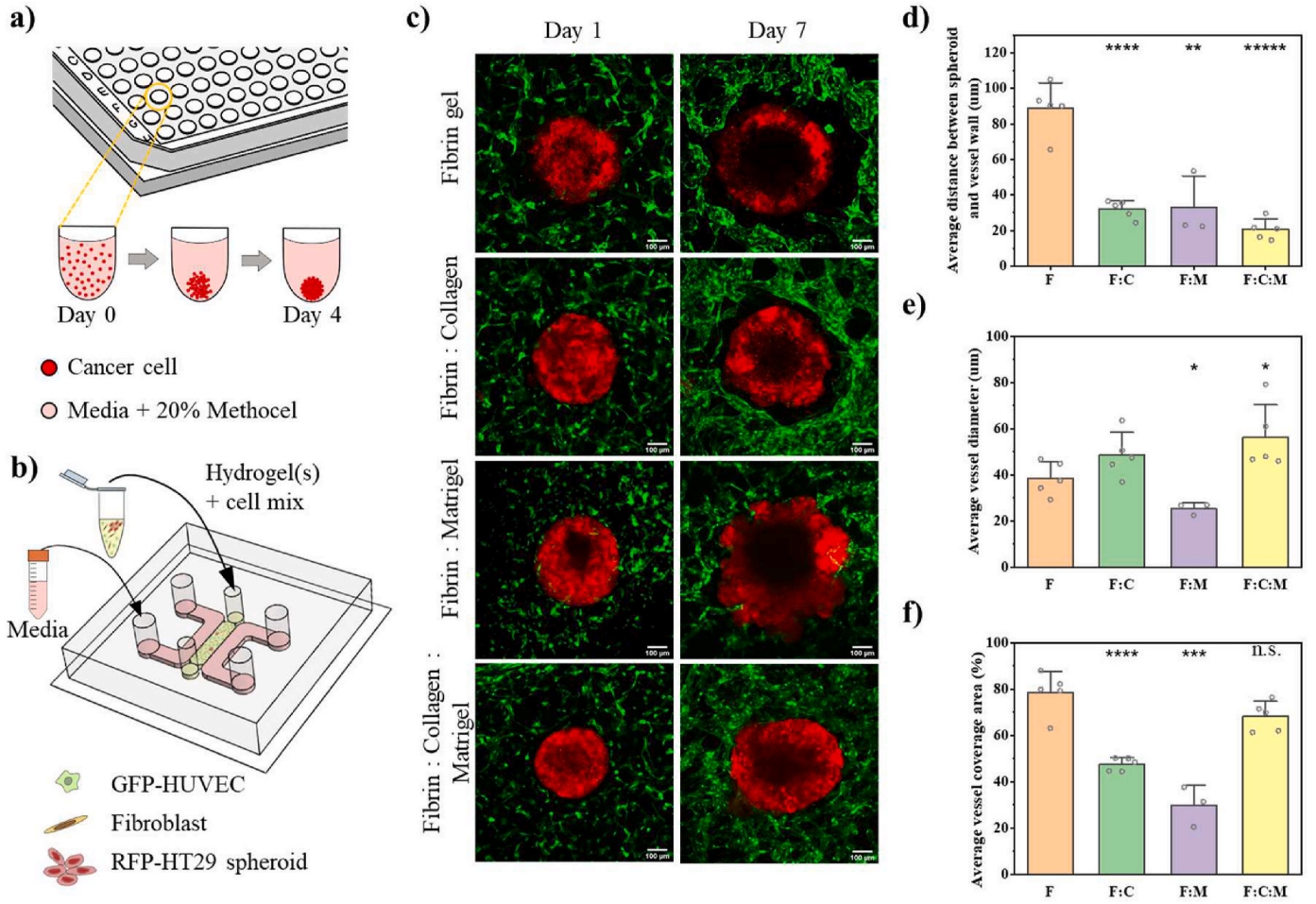

Fig. 2. Microvasculature-cancer spheroid interactions in different hydrogel combinations – a) schematic of HT-29 spheroid formation, b) encapsulation of GFP-HUVECs, fibroblasts and RFP-HT29 cancer spheroids in the microfluidic device, c) confocal images of spheroids-vasculature interactions at day 1 and day 7 post cell seeding in different hydrogel combinations, d) graph representing the average distance between the spheroid boundary and the nearest microvascular network at day 7 for different hydrogel combinations, e) plot representing the microvessel diameter encircling the tumour spheroid at day 7 for different hydrogel conditions, f) plot of average vessel coverage area around the cancer spheroids at day 7 for different hydrogel combinations. Data is represented as mean ± SD, with n = 6 for Fibrin, n = 5 for Fibrin:Collagen, n = 3 for Fibrin:Matrigel, n = 6 for Fibrin:Collagen:Matrigel over 3 independent experiments. Statistical significance was tested with student's t-test (*p< 0.05, **p<0.01, ***p<0.001, ****p<0.0001, n.s. p>0.05).

microvascular network was formed while using only Fibrin hydrogel whereas F:C:M mixture showed full integration of microvasculature and spheroid. This observation can be partly due to an increased integrin expression with the addition of collagen in fibrin hydrogel in comparison to pure fibrin matrices (Hong and Stegemann, 2008), which may lead to improved cell-ECM interactions and reduced barrier between tumour and the surrounding microvasculature. We also observed profound reduction in the vessel diameter for microvessels proximal to the tumour spheroid when compared to the microvessel diameter in the absence of tumour spheroid, in all conditions (Supplementary Fig. 3). This observation is in agreement with the literature showing that an aberrant tumour growth in the TME compresses the blood vessels leading to reduced exchange of nutrients and hypoxia (Jain et al., 2014; Helmlinger et al., 1997). These observations reinforce the major impact of composite matrices on modulating cellular functions and enhancing cellular cross-talks.

Fascinatingly, increased hydrogel complexity and the tumour spheroid-microvasculature integration, resulted in the intravasation of some tumor cells. In HT29 spheroids, we found majority of the infiltrating cells as clusters of about 3–17 cells/cluster at day 10, which is similar to intravasation dynamics reported in previous *in vitro* (Zervantonakis et al., 2012) and chicken chorioallantoic membrane (CAM) xenograft models (Stoletov et al., 2007). Interestingly, we also observed intravasation events in spheroids of size as small as 250 μm, at the time of intravasation, in accordance with a study which mentions that the onset of cancer metastasis occurs at an early stage of tumour development than is generally indicated by conventional clinical imaging of primary tumours during patient diagnosis (Deryugina and Kiosses, 2017). This further confirmed that composite matrices better recapitulate the complexity of TME. We speculate that composite matrix containing fibrin, collagen and Matrigel equips the cellular microenvironment with appropriate mechanical cues such as stiffness, porosity, and biochemical cues such as growth factors which initiates cancer cell invasion and entry into the microvessels.

It is worth mentioning that our assay was also tested for a lung cancer cell line (A549) and similar to HT29 cells, intravasation events have been observed (Supplementary Fig. 4). Observation of intravasation events in both HT29 and A549 cells validates the wider applicability of the use of composite matrices and motivates future studies to incorporate other cancer cell lines that form spheroids in our microfluidic assay with composite matrices. One limitation of this study is that while the final concentration of fibrin gel is fixed in all matrix combinations, there were variations in the final concentration of collagen and Matrigel matrices. This can explain the observed differences in vessel diameter and average vessel coverage area amongst hybrid matrices as changes in matrix composition, diameter, pore size, swelling, and stiffness are

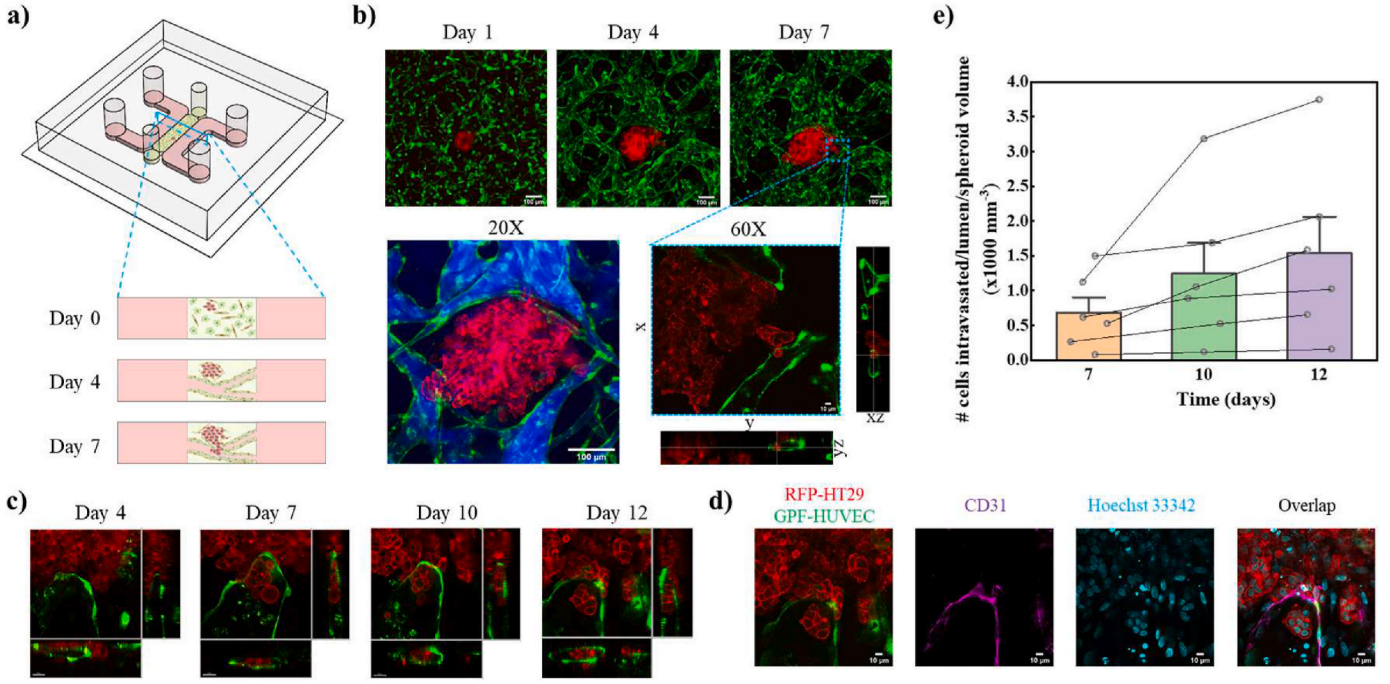

Fig. 3. Cancer cell intravasation assay – a) schematic with cross-sectional view representing time-dependent evolution of cells embedded in a Fibrin:Collagen: Matrigel hydrogel within the microfluidic device, b) time-lapse confocal microscope images (10× magnification) of HT-29 spheroid growth and microvessel formation and maturation over days. The 20X image shows the microvasculature around the spheroid is perfusable when 70 kDa blue dextran was introduced into one of the media channels. The 60X image shows the entry of cancer cells inside the microvessel lumens, confirmed through the orthogonal projections labelled as yz and xz, c) high resolution time-lapse microscopy images of cancer cells intravasation events, d) Staining of CD31 (magenta) and Hoechst33342 (cyan) in fixed samples, e) plot showing the number of intravasation events per microvessel lumen per spheroid volume. Each data point is tracked over days and connected with a line. Data is represented as mean ± SEM, with 6 spheroids in 3 independent experiments. The data across different days are not statistically significant. (For interpretation of the references to colour in this figure legend, the reader is referred to the Web version of this article.)

shown to affect cell behaviour including migration, morphology, and interactions (Ahmadzadeh et al., 2017; Schmitt et al., 2021; Stylianou et al., 2019; Kayal et al., 2020). However, even with similar individual matrix composition, it has been shown that changes in pore size, fibril diameter, and porosity in composite matrices compared to identical individual matrix composition can occur and impact cellular form and function (Anguiano et al., 2017; Malandrino and Moeendarbary, 2019; Esteki et al., 2020). Future investigation into the different ratios of F:C:M hydrogels will help identify the appropriate ratios and critical concentration of individual hydrogels for intravasation. This will give insights into understanding the role that physical cues play in the cancer cell intravasation (Micalet et al., 2021).

In summary, we report a new intravasation assay utilising the benefits of microfluidic systems, allowing the flexibility to perform parametric studies. So far, recapitulation of intravasation *in vitro* microfluidics models, has been a rare and inefficient process, possibly due to the inability to recreate the ECM. Our model overcomes this issue by integrating the tumorigenic properties of collagen and Matrigel along with fibrin hydrogels. As a result, we observed increased physical contact between different cell types, recreation of the complex tumour-stromal-vascular interactions that are necessary for cancer cells to invade, escape, and metastasise. Hence, our work emphasises the importance of the often-overlooked role played by the acellular components of the TME, whose composition influences tumour invasiveness and its crosstalk with neighbouring cells. Thus, it is essential to develop better understanding of the ECM cues that governs the behaviour of cells in a 3D environment to develop improved therapies for various diseases, in particular those dependent on matrix deposition, such as cancer and artherosclerosis (Shin et al., 2019). This study also forms a part of the ongoing effort to improve the organ-on-a-chip assays for better translatability of anti-cancer drugs.

Declaration of competing interest

The authors declare that they have no known competing financial interests or personal relationships that could have appeared to influence the work reported in this paper.

Data availability

Data will be made available on request.

Acknowledgements

We are grateful for financial support by the Wellcome Trust-MIT Fellowships to EM (WT103883), Leverhulme Trust Research Project Grant (RPG-2018-443), BBSRC (BB/V001418/1) to EM and the Cancer Research UK Multidisciplinary Award to EM (C57744/A22057). EM also recieved funding from Engineering and Physical Research Council (EP/W009889/1).

Appendix A. Supplementary data

Supplementary data to this article can be found online at https://doi.org/10.1016/j.ooc.2022.100024.

References

Ahmad, F.B., Anderson, R.N., 2021. The leading causes of death in the US for 2020. JAMA 325, 1829–1830.

Ahmadzadeh, H., et al., 2017. Modeling the two-way feedback between contractility and matrix realignment reveals a nonlinear mode of cancer cell invasion. Proc. Natl. Acad. Sci. U.S.A. 114, E1617–E1626.

Anguiano, M., et al., 2017. Characterization of three-dimensional cancer cell migration in mixed collagen-Matrigel scaffolds using microfluidics and image analysis. PLoS One. https://doi.org/10.1371/journal.pone.0171417.

Anguiano, M., et al., 2020. The use of mixed collagen-Matrigel matrices of increasing complexity recapitulates the biphasic role of cell adhesion in cancer cell migration : ECM sensing , remodeling and forces at the leading edge of cancer invasion. PLoS One 15, e0220019.
Chen, M.B., Kamm, R.D., Moeendarbary, E., 2018. Engineered models of metastasis with application to study cancer biomechanics. Adv. Exp. Med. Biol. 1092, 189–207.
Cox, T.R., 2021. The matrix in cancer. Nat. Rev. Cancer *214* **21**, 217–238, 2021.
Deryugina, E.I., Kiosses, W.B., 2017. Intratumoral cancer cell intravasation can occur independent of invasion into the adjacent stroma. Cell Rep. 19, 601–616.
Dillekås, H., Rogers, M.S., Straume, O., 2019. Are 90% of deaths from cancer caused by metastases? Cancer Med. 8, 5574–5576.
Dua, R.S., Gui, G.P.H., Isacke, C.M., 2005. Endothelial adhesion molecules in breast cancer invasion into the vascular and lymphatic systems. Eur. J. Surg. Oncol. 31, 824–832.
Ehsan, S.M., Welch-Reardon, K.M., Waterman, M.L., Hughes, C.C.W., George, S.C., 2014. A three-dimensional in vitro model of tumor cell intravasation. Integr. Biol. (Camb). 6, 603–610.
Esteki, M.H., et al., 2020. A new framework for characterization of poroelastic materials using indentation. Acta Biomater. 102, 138–148.
Fokas, E., Engenhart-Cabillic, R., Daniilidis, K., Rose, F., An, H.X., 2007. Metastasis: the seed and soil theory gains identity. Cancer Metastasis Rev. 26, 705–715.
Haase, K., Kamm, R.D., 2017. Advances in on-chip vascularization. Regen. Med. 12, 285–302.
Haase, K., et al., 2020. Endothelial regulation of drug transport in a 3D vascularized tumor model. Adv. Funct. Mater. 30, 2002444.
Han, W., et al., 2016. Oriented collagen fibers direct tumor cell intravasation. Proc. Natl. Acad. Sci. U.S.A. 113, 11208–11213.
Helmlinger, G., Yuan, F., Dellian, M., Jain, R.K., 1997. Interstitial pH and pO2 gradients in solid tumors in vivo: high-resolution measurements reveal a lack of correlation. Nat. Med. 3, 177–182.
Hong, H., Stegemann, J.P., 2008. 2D and 3D collagen and fibrin biopolymers promote specific ECM and integrin gene expression by vascular smooth muscle cells. J. Biomater. Sci. Polym. Ed. 19, 1279–1293.
Jain, R.K., Martin, J.D., Stylianopoulos, T., 2014. The role of mechanical forces in tumor growth and therapy. Annu. Rev. Biomed. Eng. 16, 321–346.
Kayal, C., Moeendarbary, E., Shipley, R.J., Phillips, J.B., 2020. Mechanical response of neural cells to physiologically relevant stiffness gradients. Adv. Healthc. Mater. 9, 1901036.
Kwaan, H.C., Lindholm, P.F., 2019. Fibrin and fibrinolysis in cancer. Semin. Thromb. Hemost. 45, 413–422.
Lai, V.K., Lake, S.P., Frey, C.R., Tranquillo, R.T., Barocas, V.H., 2012. Mechanical behavior of collagen-fibrin co-gels reflects transition from series to parallel interactions with increasing collagen content. J. Biomech. Eng. 134, 011004.
Lee, S.H., Shim, K.Y., Kim, B., Sung, J.H., 2017. Hydrogel-based three-dimensional cell culture for organ-on-a-chip applications. Biotechnol. Prog. 33, 580–589.
Li, Y.H., Zhu, C., 1999. A modified Boyden chamber assay for tumor cell transendothelial migration in vitro. Clin. Exp. Metastasis 17, 423–429.
Magdeldin, T., et al., 2017. Engineering a vascularised 3D in vitro model of cancer progression. Sci. Rep. 7, 44045.
Mak, I.W.Y., Evaniew, N., Ghert, M., 2014. Lost in translation: animal models and clinical trials in cancer treatment. Am. J. Transl. Res. 6, 114.
Malandrino, A., Moeendarbary, E., 2019. Poroelasticity of living tissues. Encycl. Biomed. Eng. 1–3, 238–245.
Meng, F., et al., 2019. 3D bioprinted in vitro metastatic models via reconstruction of tumor microenvironments. Adv. Mater. 31, 1806899.
Micalet, A., Moeendarbary, E., Cheema, U., 2021. 3D in vitro models for investigating the role of stiffness in cancer invasion. ACS Biomater. Sci. Eng. https://doi.org/10.1021/acsbiomaterials.0c01530.
Michna, R., Gadde, M., Ozkan, A., DeWitt, M., Rylander, M., 2018. Vascularized microfluidic platforms to mimic the tumor microenvironment. Biotechnol. Bioeng. 115, 2793–2806.
Naserian, S., et al., 2019. Development of bio-artificial micro-vessels with immunosuppressive capacities: a hope for future transplantations and organoids. Blood 134, 3610–3610.
Nashimoto, Y., et al., 2020. Vascularized cancer on a chip: the effect of perfusion on growth and drug delivery of tumor spheroid. Biomaterials 229, 119547.
Roberts, A.B., et al., 2021. Tumor cell nuclei soften during transendothelial migration. J. Biomech. 121, 110400.
Schmitt, T., et al., 2021. Vitro characterization of xeno-free clinically relevant human collagen and its applicability in cell-laden 3D bioprinting. J. Biomater. Appl. 35, 912–923.
Shin, Y., et al., 2019. Emulating endothelial dysfunction by implementing an early atherosclerotic microenvironment within a microfluidic chip. Lab Chip 19, 3664–3677.
Stoletov, K., Montel, V., Lester, R.D., Gonias, S.L., Klemke, R., 2007. High-resolution imaging of the dynamic tumor cell-vascular interface in transparent zebrafish. Proc. Natl. Acad. Sci. U.S.A. 104, 17406–17411.
Stylianou, A., Gkretsi, V., Louca, M., Zacharia, L.C., Stylianopoulos, T., 2019. Collagen content and extracellular matrix cause cytoskeletal remodelling in pancreatic fibroblasts. J. R. Soc. Interface 16.
Tacconi, C., et al., 2022. KIT is dispensable for physiological organ vascularisation in the embryo. Angiogenesis 25, 343–353.
Whelan, I.T., Moeendarbary, E., Hoey, D.A., Kelly, D.J., 2021. Biofabrication of vasculature in microphysiological models of bone. Biofabrication 13.
Ye, T., Qiu, F., 2019. Influence of matrigel on the shape and dynamics of cancer cells. Chin. Phys. B 28.
Zervantonakis, I.K., et al., 2012. Three-dimensional microfluidic model for tumor cell intravasation and endothelial barrier function. Proc. Natl. Acad. Sci. USA 109, 13515–13520.